Toward Resilient Solar-Integrated Distribution Grids: Harnessing the Mobility of Power Sources

Zijiang Yang, *Student Member, IEEE*, Mostafa Nazemi, *Student Member, IEEE,*
Payman Dehghanian, *Member, IEEE*, and Masoud Barati, *Senior Member, IEEE*

***Abstract*—In the past decades, weather- and cyber-driven high-impact low-probability (HILP) disasters have been observed more frequently. Mobile power sources (MPSs) including truck-mounted mobile emergency generators, mobile energy storage systems, and electric vehicles have a great potential for enhancing the power system resilience. This paper mainly focuses on investigating the potential roles of the MPS in facilitating a swift restoration of power distribution systems when facing HILP disasters. The distribution system reconfiguration through real-time topology changes is also taken into account to best utilize the network built-in flexibility and help power delivery during emergencies. A mixed-integer nonlinear programming model is proposed for deriving a solution for MPS dispatch and distribution system reconfiguration under a given repair strategy. The model is further linearized into a tractable mix-integer linear programming formulation. Eventually, the coordination of the proposed MPS and photovoltaic (PV) generation is investigated.**

***Index Terms*—Distribution systems (DS); high-impact low-probability (HILP) hazards; mobile power sources (MPS); routing and scheduling; solar generation; dynamic reconfiguration.**

NOMENCLATURE

A. Sets and Indices

$i, j \in \mathbf{B}$	Indices/set of nodes.
$m \in \mathbf{M}$	Index/set of mobile power sources (MPSs).
$t, \tau \in \mathbf{T}$	Indices/set of time periods.
$(i, j) \in \mathbf{L}$	Indices/set of network branches.
$N_{\mathbf{B}}, N_{\mathbf{T}}, N_{\mathbf{L}}$	Number of all nodes, time periods, branches.
$\mathbf{B}^{\text{sub}}$	Set of substation nodes.
$\mathbf{B}_m$	Set of candidate nodes that can be connected to MPS m.
$\mathbf{B}_t^{\text{S}}$	Set of selected source nodes for the fictitious flows at time t.
$\mathbf{L}^{\text{sw}}$	set of branches equipped with remotely-controlled switches (RCSs).
$\mathbf{L}_t^{\text{D}}$	Set of branches that are damaged and have not been repaired at time t.
$\mathbf{G} \in \mathbf{M}$	Set of mobile emergency generators (MEGs).
$\mathbf{S} \in \mathbf{M}$	Set of mobile energy storage systems (MESSs).
$\mathbf{V} \in \mathbf{M}$	Set of mobile electric vehicle (EV) fleets.
$\mathbf{M_i}$	Set of MPSs that can be connected to node i.

B. Parameters and Constants

χ_i	Priority of the load demanded at node i.
$\beta_{ij,t}$	Binary damage status of branch (i, j) at time t (1 if the branch is undamaged or has been repaired, 0 otherwise).
$P_{i,t}^{\text{de}}$	Real power demand of node i at time t (kW).
$Q_{i,t}^{\text{de}}$	Reactive power demand of node i at time t (kVar).
α_{ij}^0	Binary parameter representing the initial status of branch (i,j) (1 if the branch is connected, 0 otherwise).
N_t^{I}	Number of islands due to the damaged and unrepaired branches at time t.
N_i^{mps}	Number of MPSs that are allowed to be connected to node i.
$T_{m,ij}^{\text{tr}}$	Travel time of MPS m from node i to node j.
Δt	Duration of one time period.
M	A large-enough positive number.
$\underline{\text{SOC}}_m$	Minimum state of charge (SOC) of MESS or EV fleet m (kWh).
$\overline{\text{SOC}}_m$	Maximum SOC of the MESS or EV fleet m.
$\overline{P}_m^{\text{ch}}, \overline{P}_m^{\text{dch}}$	Maximum charging and discharging power of MESS or EV fleet m (kW, kVar).
$\overline{P}_m, \overline{Q}_m$	Maximum real and reactive power output of MPS m (kW, kVar).
$\overline{P}_{ij}, \overline{Q}_{ij}$	Real and reactive power capacity of branch (i, j) (kW, kVar).
r_{ij}, x_{ij}	Resistance and reactance of branch (i, j) (Ω).
$\underline{\text{Vsq}}_i$	Minimum squared voltage magnitude at node i (kV^2).
$\overline{\text{Vsq}}_i$	Maximum squared voltage magnitude at node i (kV^2).
C_m^{tr}	Transportation cost coefficient of MPS m.
C_m^{P}	Power rating price of MESS or EV fleet m (\$/kWh).
k_m	Degradation slope of MESS or EV fleet m.
δ_m	Generation cost coefficient of MEG m.
$\eta_m^{\text{ch}}, \eta_m^{\text{dch}}$	Charging and discharging efficiency of MESS or EV fleet m.
P_m^{tr}	Energy Consumption rate of EV fleet m when

Z.Yang, M. Nazemi, and P. Dehghanian are with the Department of Electrical and Computer Engineering, George Washington University, Washington, DC 20052, USA (e-mails: zyang55@gwu.edu; mostafa_nazemi@gwu.edu; payman@gwu.edu).

M. Barati is with the Department of Electrical and Computer Engineering, University of Pittsburgh, Pittsburgh, PA 15261, USA (e-mail: masoud.barati@pitt.edu).

978-1-7281-4547-1/20/$31.00 ©2020 IEEE

traveling (kW).

$d^{\text{fic}}_{i,t}$ Fictitious load of node i at time t.

PVC Value of loss of solar energy ($/kWh)

$\overline{P}^{s}_{i,t}$ Maximum available real power from solar farm connected to node i at time t (kW)

C. Functions and Variables

$pd_{i,t}, qd_{i,t}$ Real and reactive power demand supplied at node i at time t (kW, kVar).

$pg_{i,t}, qg_{i,t}$ Real and reactive power at substation node i at time t (kW, kVar).

$pf_{ij,t}, qf_{ij,t}$ Real and reactive power flow on branch (i, j) at time t (kW, kVar).

$\text{SOC}_{m,t}$ SOC of MESS or EV fleet m at time t (kWh).

$p^{\text{ch}}_{m,t}, p^{\text{dch}}_{m,t}$ Charging and discharging power of MESS or EV fleet m at time t (kW).

$p_{m,t}, q_{m,t}$ Real and reactive power output of MPS m at time t (kW, kVar).

$p^{\text{mps}}_{i,t}, q^{\text{mps}}_{i,t}$ Real and reactive power output of MPS at node i at time t (kW, kVar).

$Vsq_{i,t}$ Squared voltage magnitude at node i at time t (kV^2).

$fl_{ij,t}$ Fictitious flow on branch (i, j) at time t.

$fg_{i,t}$ Fictitious supply at source node i at time t.

$p^{\text{SC}}_{i,t}$ Curtailed power of solar farm connected to node i at time t (kW).

$p^{s}_{i,t}$ Real power generated by solar farm connected to node i at time t (kW).

D. Binary Variables

$\alpha_{ij,t}$ Connection status of branch (i, j) at time t (1 if the branch is connected, 0 otherwise).

$c_{m,t}, d_{m,t}$ Charging and discharging status of MESS or EV fleet m at time t (1 if it is charging or discharging; 0 otherwise).

$\varphi_{m,t}$ Traveling status of MPS m at time t (1 if the MPS is traveling; 0 otherwise).

$\mu_{m,i,t}$ Connection status of MPS m to node i at time t (1 if connected; 0 otherwise).

I. Introduction

In the recent years, more frequent realization of the high-impact low-probability (HILP) hazards and catastrophes has resulted in prolonged electricity outages, excessive equipment damages, and severe economic losses in our modern society [1]. Power system resilience to HILP events can be elevated by harnessing the network topology [2], advanced control solutions [3], and deployment of additional flexibility to harness the procured spinning reserve services [4]. Mobile power sources (MPSs), including truck-mounted emergency generators (MEGs), mobile energy storage systems (MESSs), and electric vehicles (EVs) have great potentials to be employed as grid-support resources during emergency operating conditions to supply the critical loads and enhance the resilience of the distribution system (DS). This is achieved via a swift disaster restoration. Due to the evolving battery technology and the increasing demand for a more resilient power system, the application of MPS in microgrids has been recently of interest.

Deployment of MPSs for enhanced resilience of DS has been studied in several research efforts [5]–[7]. In [8], and to minimize the post-disaster restoration cost, the MESS and DS network reconfiguration is coordinated via a MILP model to facilitate the service restoration to critical loads. MESSs can transfer the energy among multiple microgrids in the DS by traveling to and locating at different locations in proper time. Proactive preparedness prior to an imminent hurricane is investigated in [9], including the allocation of generation resources (i.e. diesel oil, electric batteries, and electric buses) in the system that incorporates distributed generators, microgrids, charging stations and critical loads. EVs can be charged to store energy not only to meet their own transportation requirements, but also as an emergency power source to supply electricity to critical loads during emergencies. The impact of vehicle to grid (V2G) services both on the individual EV and the power system operation is studied in [10].

In this paper, the potential of MPSs for DS restoration following natural disasters is investigated. In addition, the coordination of photovoltaic (PV) generation with MPSs is explored to verify how the joint coordination can improve the network resilience.

II. Problem Formulation

This section presents an extensive formulation for routing and scheduling of MPS. Motivated by [11], the objective function (1) includes five terms, as follows:

$$\begin{aligned}\max\Big(&\sum_{t\in\mathbf{T}}\sum_{i\in\mathbf{B}}\chi_i\cdot pd_{i,t}-\sum_{t\in\mathbf{T}}\sum_{m\in\mathbf{M}}C^{\text{tr}}_m\cdot\varphi_{m,t}\\&-\sum_{t\in\mathbf{T}}\sum_{m\in\{\mathbf{S},\mathbf{V}\}}C^{\text{P}}_m\cdot(p^{\text{ch}}_{m,t}+p^{\text{dch}}_{m,t})-\\&\sum_{t\in\mathbf{T}}\sum_{m\in\mathbf{G}}\delta_m\cdot p_{m,t}-\sum_{t\in\mathbf{T}}\sum_{i\in\mathbf{B}}\text{PVC}\cdot p^{\text{SC}}_{i,t}\Big)\end{aligned}\tag{1}$$

The first term is the total loads supplied, weighted by the priority of the load points χ_i, i.e., the weighted sum of supplied loads, over the entire restoration time period $\mathbf{T}$; the second term is the transportation cost of MPSs, due to the trips they make during the restoration phases; the third term reflects the cost of EV fleet and MESSs battery degradation when charging and discharging during the restoration process; and the last term is the relative cost of the MEG outputs. The second term is added to minimize the traveling time of MPSs and avoid unnecessary transportation since the MPSs should not travel around once all loads are restored. Meanwhile, if there may exist various MPS dispatch strategies that can achieve the same restoration result, the optimal strategy with minimum transportation cost will be selected. The third term is aimed to reduce the battery degradation cost so that the redundant charging and discharging are avoided during the restoration phases. The MEGs consume fuel to generate power and provide the energy for their transportation. The forth term is added to minimize the costs associated with the power output of MEGs so that the unnecessary real power output from MEGs is reduced. Additionally, if there are multiple

MEGs with different generation cost (represented by δ_m) available for dispatch, the strategy with lower generation cost is selected. The last term is represented by the value of loss of solar energy multiplied by the curtailed power of solar farm during the restoration process. This term is added to minimizing the cost resulted by the curtailed solar so that the use of solar energy is maximized.

Along with this objective, a number of constraints need to be considered for the DS restoration problem as follows.

1) MPS Connection Constraints: Following a HILP disaster, the MPSs rapidly travel and get connected in physical islands (PIs) to supply electricity where needed. At each time period, MPS can be connected to at most one pre-determined candidate node, as enforced in (2). MPSs cannot connect to the load points that are not equipped with associated facilities, as stated in constraint (3). Constraint (4) indicates that the allowed number of MPSs connected to a node is limited to stations' capacity at each candidate node. Constraint (5) states that the MPSs cannot travel to other nodes when connected to a candidate node.

$$\sum_{i\in\mathbf{B}_m}\mu_{m,i,t}\le 1,\forall m\in\mathbf{M},\forall t\in\mathbf{T} \tag{2}$$

$$\sum_{i\in\mathbf{B}\backslash\mathbf{B}_m}\mu_{m,i,t}=0,\ \forall m\in\mathbf{M},\forall t\in\mathbf{T} \tag{3}$$

$$\sum_{m\in\mathbf{M}_i}\mu_{m,i,t}\le N_i^{\text{mps}},\forall i\in\bigcup_{m\in\mathbf{M}}\mathbf{B}_m,\forall t\in\mathbf{T} \tag{4}$$

$$\varphi_{m,t}=1-\sum_{i\in\mathbf{B}_m}\mu_{m,i,t},\forall m\in\mathbf{M},\forall t\in\mathbf{T} \tag{5}$$

2) MPS Routing Constraints: constraint (6) ensures that the MPSs transportation among different DS nodes satisfies the required travel time.

$$\begin{aligned}&\mu_{m,i,t+\tau}+\mu_{m,j,t}\le 1,\\&\forall m\in\mathbf{M},\ \forall i,j\in\mathbf{B}_m,\ \forall\tau\le T_{m,ij}^{\text{tr}},\ \forall t+\tau\le N_{\mathbf{T}}\end{aligned} \tag{6}$$

3) MPS Power Scheduling Constraints: It is assumed that the trunk-mounted MESS and MEG can be refueled for transportation during the restoration process [12], while EVs consume electric energy when they are in transport. The change in the state of charge (SOC) of MESSs over time is determined by their charging and discharging behaviors, as represented in (7) while the SOC of EVs is determined by their charging and discharging as well as travel behaviors (8). Constraint (9) restricts the range of SOC of MESS and EV over all time periods. Constraint (10) and (11) respectively impose the range of charging and discharging power for MESS and EV according to the corresponding rated power. The charging and discharging power are both enforced to be zero when MESS and EV are not connected to the DS. Charging and discharging of MESS and EV are mutually exclusive over all time periods, as represented in (12) which indicates that the MPS disconnected from DS can neither charge nor discharge. Constraint (13) and (14) set the MEG real and reactive power output limits, respectively, and enforce MEG to have zero real and reactive output when it is disconnected from DS.

$$\begin{aligned}\text{SOC}_{m,t}=\text{SOC}_{m,t-1}+(\eta_m^{\text{ch}}\cdot p_{m,t}^{\text{ch}}-p_{m,t}^{\text{dch}}/\eta_m^{\text{dch}}\cdot\\ \forall m\in\mathbf{S},\ \forall t\ge 1\end{aligned} \tag{7}$$

$$\begin{aligned}\text{SOC}_{m,t}=\text{SOC}_{m,t-1}+(\eta_m^{\text{ch}}\cdot p_{m,t}^{\text{ch}}-p_{m,t}^{\text{dch}}/\eta_m^{\text{dch}}-\\ \varphi_{m,t}\cdot P_m^{\text{tr}})\cdot\Delta t,\qquad\forall m\in\mathbf{V},\ \forall t\ge 1\end{aligned} \tag{8}$$

$$\underline{\text{SOC}}_m\le\text{SOC}_{m,t}\le\overline{\text{SOC}}_m,\forall m\in\{\mathbf{S},\mathbf{V}\},\forall t\in\mathbf{T} \tag{9}$$

$$0\le p_{m,t}^{\text{ch}}\le c_{m,t}\cdot\overline{P}_m^{\text{ch}},\forall m\in\{\mathbf{S},\mathbf{V}\},\forall t\in\mathbf{T} \tag{10}$$

$$0\le p_{m,t}^{\text{dch}}\le d_{m,t}\cdot\overline{P}_m^{\text{dch}},\forall m\in\{\mathbf{S},\mathbf{V}\},\forall t\in\mathbf{T} \tag{11}$$

$$c_{m,t}+d_{m,t}\le\sum_{i\in\mathbf{B}_m}\mu_{m,i,t},\forall m\in\{\mathbf{S},\mathbf{V}\},\forall t\in\mathbf{T} \tag{12}$$

$$0\le p_{m,t}\le\sum_{i\in\mathbf{B}_m}\mu_{m,i,t}\cdot\overline{P}_m,\forall m\in\mathbf{G},\forall t\in\mathbf{T} \tag{13}$$

$$0\le q_{m,t}\le\sum_{i\in\mathbf{B}_m}\mu_{m,i,t}\cdot\overline{Q}_m,\forall m\in\mathbf{G},\forall t\in\mathbf{T} \tag{14}$$

4) DS Radiality Constraints: Constraints (15)-(18) ensure that the DS remains radial over all time periods. For DS radiality, there are two conditions which need to be satisfied: (i) at each PI, the number of connected branches is equal to the total number of nodes in the PI - 1; (ii) all load points are connected to a determined source node in each PI. The first condition is satisfied in constraint (15). In each PI, one node is considered as a fictitious source node and the remaining nodes are fictitious load points. The fictitious source node and fictitious load node are the source and the destination of fictitious power flow, respectively. The amount of the fictitious flow into a load node $d_{i,t}^{\text{fic}}$ is set as 1 at all nodes. The second condition is satisfied in constraint (16)-(18) that enforce each load node to receive one unit of the fictitious flow from the fictitious source node at each PI. Constraints (16)-(17) ensure the fictitious flow balance for the fictitious load and source nodes, respectively. Constraint (18) enforces the fictitious flow to be zero in open branches. The large enough positive number M relaxes this constraint when some branches are open (See [13] for additional details on the fictitious network and radiality conditions).

$$\sum_{(i,j)\in\mathbf{L}}\alpha_{ij,t}=N_{\mathbf{B}}-N_t^{\text{I}},\forall t\in\mathbf{T} \tag{15}$$

$$\sum_{(j,i)\in\mathbf{L}}fl_{ji,t}-\sum_{(i,j)\in\mathbf{L}}fl_{ij,t}=d_{i,t}^{\text{fic}},\forall i\in\mathbf{B}\backslash\mathbf{B}_t^{\text{S}},\forall t\in\mathbf{T} \tag{16}$$

$$\sum_{(i,j)\in\mathbf{L}}fl_{ij,t}-\sum_{(j,i)\in\mathbf{L}}fl_{ji,t}=fg_{i,t},\forall i\in\mathbf{B}_t^{\text{S}},\forall t\in\mathbf{T} \tag{17}$$

$$-\alpha_{ij,t}\cdot M\le fl_{ij,t}\le\alpha_{ij,t}\cdot M,\forall(i,j)\in\mathbf{L},\forall t\in\mathbf{T} \tag{18}$$

5) Branch Status Constraints: According to (19), the damaged branch must be open if it has not yet been repaired at time t. Constraint (20) states that the undamaged branches without RCS remain in their initial status over all time periods.

$$\alpha_{ij,t}\le\beta_{ij,t},\forall(i,j)\in\mathbf{L},\forall t\in\mathbf{T} \tag{19}$$

$$\alpha_{ij,t}=\alpha_{ij}^0,\forall(i,j)\in\mathbf{L}\backslash\{\mathbf{L}_t^{\text{D}},\mathbf{L}^{\text{sw}}\},\forall t\in\mathbf{T} \tag{20}$$

6) MPS Output Power Constraints: Constraints (21)-(22) indicate that the real or reactive power injection or extraction at a candidate node for MPS is equal to the sum of the real or

reactive power output of the MPSs. The non-MPS nodes have zero real and reactive power from MPSs as expressed in (23).

$$p_{i,t}^{\text{mps}} = \sum_{m\in\mathbf{M}_i\cap\{\mathbf{S},\mathbf{V}\}} \mu_{m,i,t}\cdot p_{m,t}^{\text{dch}} - \sum_{m\in\mathbf{M}_i\cap\{\mathbf{S},\mathbf{V}\}} \mu_{m,i,t}\cdot p_{m,t}^{\text{ch}} + \sum_{m\in\mathbf{M}_i\cap\mathbf{G}} \mu_{m,i,t}\cdot p_{m,t}, \quad \forall i\in \bigcup_{m\in\mathbf{M}}\mathbf{B}_m, \forall t\in\mathbf{T} \tag{21}$$

$$q_{i,t}^{\text{mps}} = \sum_{m\in\mathbf{M}_i} \mu_{m,i,t}\cdot q_{m,t}, \quad \forall i\in \bigcup_{m\in\mathbf{M}}\mathbf{B}_m, \forall t\in\mathbf{T} \tag{22}$$

$$p_{i,t}^{\text{mps}} = q_{i,t}^{\text{mps}} = 0, \quad \forall i\in \mathbf{B}\backslash \bigcup_{m\in\mathbf{M}}\mathbf{B}_m, \forall t\in\mathbf{T} \tag{23}$$

7) Power Balance Constraints: Constraints (24)-(25) describe the real and reactive power balance conditions at all nodes, respectively. Note that it is assumed here that the power factor of the PV generation is 1, and thus the PV farm only injects real power into the distribution grid. The solar power curtailment is formulated in constraint (26). At any node hosting the solar farm, the solar power generation depends on solar availability and solar power capacity as demonstrated in constraint (27). The range of the demanded load to be supplied is bounded in constraint (28). Constraint (29) enforces the recovery rate of the supplied loads not to decrease. The demand power factor is assumed to be fixed in (30). The real and reactive power flows in online branches are respectively limited by their real and reactive power capacities in (31)-(32). Constraints (31)-(32) also enforce the real and reactive power flow in open branches to be zero.

$$\sum_{(j,i)\in\mathbf{L}} pf_{ji,t} - \sum_{(i,j)\in\mathbf{L}} pf_{ij,t} = pd_{i,t} - pg_{i,t} - p_{i,t}^{\text{mps}} - p_{i,t}^{s}, \quad \forall i\in\mathbf{B}, \forall t\in\mathbf{T} \tag{24}$$

$$\sum_{(j,i)\in\mathbf{L}} qf_{ji,t} - \sum_{(i,j)\in\mathbf{L}} qf_{ij,t} = qd_{i,t} - qg_{i,t} - q_{i,t}^{\text{mps}}, \quad \forall i\in\mathbf{B}, \forall t\in\mathbf{T} \tag{25}$$

$$p_{i,t}^{\text{SC}} = \overline{P}_{i,t}^{s} - p_{i,t}^{s}, \quad \forall i\in\mathbf{B}, \forall t\in\mathbf{T} \tag{26}$$

$$0 \le p_{i,t}^{s} \le \overline{P}_{i,t}^{s}, \quad \forall i\in\mathbf{B}, \forall t\in\mathbf{T} \tag{27}$$

$$0 \le pd_{i,t} \le P_{i,t}^{\text{de}}, \forall i\in\mathbf{B}, \ \forall t\in\mathbf{T} \tag{28}$$

$$pd_{i,t-1}/P_{i,t-1}^{\text{de}} \le pd_{i,t}/P_{i,t}^{\text{de}}, \forall i\in\mathbf{B}, \ \forall t\ge 1 \tag{29}$$

$$qd_{i,t} = (Q_{i,t}^{\text{de}}/P_{i,t}^{\text{de}})\cdot pd_{i,t}, \forall i\in\mathbf{B}, \ \forall t\in\mathbf{T} \tag{30}$$

$$-\alpha_{ij,t}\cdot\overline{P}_{ij} \le pf_{ij,t} \le \alpha_{ij,t}\cdot\overline{P}_{ij}, \forall (i,j)\in\mathbf{L}, \forall t\in\mathbf{T} \tag{31}$$

$$-\alpha_{ij,t}\cdot\overline{Q}_{ij} \le qf_{ij,t} \le \alpha_{ij,t}\cdot\overline{Q}_{ij}, \forall (i,j)\in\mathbf{L}, \forall t\in\mathbf{T} \tag{32}$$

8) Power Flow Constraints: Constraint (33) and (34) represent the power flow equation in which the M value is a relaxation parameter. Constraint (35) states the boundary for the voltage magnitudes.

$$Vsq_{i,t} - Vsq_{j,t} \le (1-\alpha_{ij,t})\cdot M + 2\cdot(r_{ij}\cdot pf_{ij,t} + x_{ij}\cdot qf_{ij,t}), \quad \forall (i,j)\in\mathbf{L}, \forall t\in\mathbf{T} \tag{33}$$

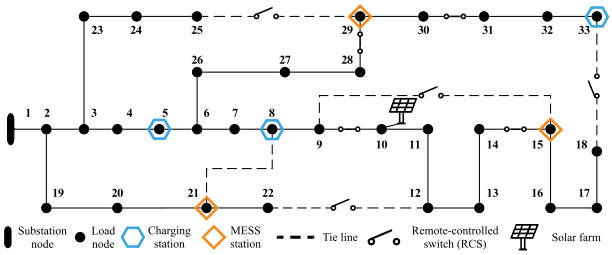

Fig. 1. The modified IEEE 33-node test system with solar farms.

$$Vsq_{i,t} - Vsq_{j,t} \ge (\alpha_{ij,t}-1)\cdot M + 2\cdot(r_{ij}\cdot pf_{ij,t} + x_{ij}\cdot qf_{ij,t}), \quad \forall (i,j)\in\mathbf{L}, \forall t\in\mathbf{T} \tag{34}$$

$$\underline{\text{Vsq}}_i \le Vsq_{i,t} \le \overline{\text{Vsq}}_i, \forall i\in\mathbf{B}, \forall t\in\mathbf{T} \tag{35}$$

Note that constraints (21) and (22) include non-linear terms making the optimization problem a mixed-integer non-linear programming (MINLP) model. We propose a linearization technique as illustrated below [14]:

$$0 \le P_{m,i,t}^{\text{dch}} \le \mu_{m,i,t}\cdot\overline{P}_{m}^{\text{dch}} \tag{36}$$

$$p_{m,t}^{\text{dch}} + (\mu_{m,i,t}-1)\cdot\overline{P}_{m}^{\text{dch}} \le P_{m,i,t}^{\text{dch}} \le p_{m,t}^{\text{dch}} \tag{37}$$

where, if $\mu_{m,i,t}=1$, then we have $P_{m,i,t}^{\text{dch}} = p_{m,t}^{\text{dch}}$; if $\mu_{m,i,t}=0$, then $P_{m,i,t}^{\text{dch}} = 0$. The MINLP formulation is hence linearized into a mixed-integer linear programming (MILP) problem and, therefore, the computation complexity is reduced.

III. Numerical Results and Discussions

In order to verify the effectiveness, the proposed method is applied to a modified IEEE 33-node test system which contains one substation node and 37 distribution lines (including 5 tie lines). All simulations are executed in GAMS software on a Laptop with Intel CoreTM i7 CPU @ 3.40 GHz and 8 GB RAM. We here assume that the stations with grid connection facilities for EV fleets are charging stations and the stations with grid connection facilities for MESSs and MEGs are designated as the MESS stations. Furthermore; it is also assumed that a PV farm of 500 kW capacity is located at node 10 as 1 demonstrates. Besides, we assume there are 3 charging stations and 3 MESS stations available in the DS. Additionally, 8 RCSs are allocated; 3 MPSs are available: MESS 1 with 500 kW/776 kWh, MEG 1 with 800 kW/600 kVar, and EV fleet 1 incorporating 2 electric buses with 150 kW/150 kWh capacity and 0.25 kW energy consumption rate for transportation. The tie lines in the DS are normally open. Only the branches equipped with RCS can be switched during the restoration process. The connection status of tie lines are open while the rest branches are closed during normal operation. All MPSs are located at the substation node and fully charged to prepare for potential emergency events. When an emergency event occurs, and once the damaged branches are identified and the repair plan is generated, the MPSs will depart from the substation node to supply the critical loads across the DS.

It is assumed that 8 branches are damaged following a HILP event. The repair schedule for damaged branches is taken as follows: branch 16-17 at *t*=3, branch 11-12 at *t*=7, branch 29-30 at *t*=12, branch 27-28 at *t*=14, branch 6-26 at *t*=16, branch

TABLE I
LOCATION OF MPSS IN EACH TIME PERIOD WITH PV GENERATION

---		Time Period								
		1	2	3	4~5	6	7	8~12	13~14	15~24
MPS	EV 1	node 1	→		node 8		→	node 33	→	node 8
	MESS 1	node 1	→		node 15		→	node 29		
	MEG 1	node 1	→		node 15					

TABLE II
DISTRIBUTION SYSTEM (DS) RECONFIGURATION ACTIONS

Time period	Remote-controlled switch (RCS) actions
t = 1	close branch 9-15, 12-22, 18-33, 25-29
t = 7	open branch 14-15
t = 18	open branch 18-33
t = 20	close branch 14-15, open branch 9-15, 25-29
t = 24	open branch 12-22

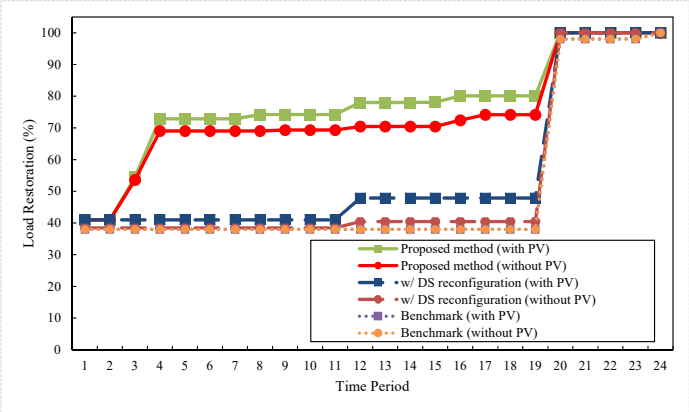

Fig. 2. Load restoration in each time period with different strategies.

6-7 at t=18, branch 4-5 at t=20, and branch 21-22 at t=24. Accordingly, the total restoration period is set as $N_{\mathbf{T}}$ = 24 time periods where each time period lasts $\Delta t = 0.5hr$.

The proposed MPS dispatch method is exploited to both systems with and without PV farms. The MPS dispatch strategy for the DS considering a PV farm at bus 10 is obtained and illustrated in Table I. Note that the symbol "→" denotes the MPS in transportation mode. The optimal RCS actions for both systems with and without PV generation are found the same, as shown in Table II. The recovery rate achieved in both cases (with and without PV generation) in each time period is depicted in Fig. 2. Different scenarios including and excluding DS reconfiguration as well as the benchmark case indicating the system without MPSs and DS reconfiguration are illustrated in Fig. 2 for comparison. As can be seen, the benchmark scenario has the lowest recovery rate over the restoration process. The proposed MPS dispatch method coordinated with PV generation improves the recovery rate around 7% higher than that in the case without PV generation at $t = 12 \sim 16$. One can conclude that the coordination of PV generation in DS with the applied MPS routing and scheduling mechanism can have a significant contribution to DS restoration and resilience.

IV. CONCLUSION

This paper proposed a mechanism for coordination of MPSs routing and scheduling with PV generation to improve the DS operational resilience in dealing with the aftermath of HILP disasters. The original MINLP model is reformulated to a MILP counterpart to attain a structured coherent strategy in solar-integrated DS that harnesses the full potential of MPSs to accelerate the load outage recovery. Numerical results demonstrated that the proposed methodology could effectively facilitate the DS restoration, resulting in a remarkable reduction in the outage duration and enhanced operational resilience.

Future research should encapsulate some practical considerations for real-world implementations. One may consider and integrate into the model (i) the transportation accessibility limitations due to the damaged roads, highways, and bridges, or (ii) PV generation restrictions during HILP events (day or days after) due to either being damaged by a HILP event or being covered by snow or cloud shadows. Future research may take into account such realistic constraints that may prevent otherwise its practical application and usefulness.

REFERENCES

[1] M. Nazemi, M. Moeini-Aghtaie, M. Fotuhi-Firuzabad, and P. Dehghanian, "Energy storage planning for enhanced resilience of power distribution networks against earthquakes," *IEEE Transactions on Sustainable Energy*, 2019.

[2] M. Nazemi, P. Dehghanian, and M. Lejeune, "A mixed-integer distributionally robust chance-constrained model for optimal topology control in power grids with uncertain renewables," *13th IEEE Power and Energy Society (PES) PowerTech Conference*, 2019.

[3] W. Shiyuan, P. Dehghanian, M. Alhazmi, and M. Nazemi, "Advanced control solutions for enhanced resilience of modern power-electronic-interfaced distribution systems," *Journal of Modern Power Systems and Clean Energy*, pp. 1–15, 2019.

[4] M. Khoshjahan, P. Dehghanian, M. Moeini-Aghtaie, and M. Fotuhi-Firuzabad, "Harnessing ramp capability of spinning reserve services for enhanced power grid flexibility," *IEEE Transactions on Industry Applications*, 2019.

[5] S. Lei, C. Chen, Y. Li, and Y. Hou, "Resilient disaster recovery logistics of distribution systems: Co-optimize service restoration with repair crew and mobile power source dispatch," *IEEE Trans. on Smart Grid*, 2019.

[6] B. Wang, J. A. Camacho, G. M. Pulliam, A. H. Etemadi, and P. Dehghanian, "New reward and penalty scheme for electric distribution utilities employing load-based reliability indices," *IET Generation, Transmission & Distribution*, vol. 12, no. 15, pp. 3647–3654, 2018.

[7] S. Lei, C. Chen, H. Zhou, and Y. Hou, "Routing and scheduling of mobile power sources for distribution system resilience enhancement," *IEEE Transactions on Smart Grid*, 2018.

[8] S. Yao, P. Wang, and T. Zhao, "Transportable energy storage for more resilient distribution systems with multiple microgrids," *IEEE Transactions on Smart Grid*, 2018.

[9] H. Gao, Y. Chen, S. Mei, S. Huang, and Y. Xu, "Resilience-oriented pre-hurricane resource allocation in distribution systems considering electric buses," *Proceedings of the IEEE*, vol. 105, no. 7, pp. 1214–1233, 2017.

[10] Y. Ma, T. Houghton, A. Cruden, and D. Infield, "Modeling the benefits of vehicle-to-grid technology to a power system," *IEEE Transactions on power systems*, vol. 27, no. 2, pp. 1012–1020, 2012.

[11] Z. Yang, P. Dehghanian, and M. Nazemi, "Enhancing seismic resilience of electric power distribution systems with mobile power sources," *EEE Industry Applications Society (IAS) Annual Meeting*, 2019.

[12] S. Iwai, T. Kono, M. Hashiwaki, and Y. Kawagoe, "Use of mobile engine generators as source of back-up power," in *31st International Telecommunications Energy Conference (INTELEC)*, pp. 1–6, 2009.

[13] M. Lavorato, J. F. Franco, M. J. Rider, and R. Romero, "Imposing radiality constraints in distribution system optimization problems," *IEEE Transactions on Power Systems*, vol. 27, no. 1, pp. 172–180, 2012.

[14] W. Wei, F. Liu, S. Mei, and Y. Hou, "Robust energy and reserve dispatch under variable renewable generation," *IEEE Transactions on Smart Grid*, vol. 6, no. 1, pp. 369–380, 2015.